Delineation of the exposure-response causality chain of chronic copper toxicity to the zebra mussel, Dreissena polymorpha, with a TK-TD model based on concepts of biotic ligand model and subcellular metal partitioning model

Le, T.T.Y.; Milen, N.; Grabner, D.; Hendriks, A.J.; Peijnenburg, W.J.G.M.; Sures, B.

Chemosphere 286 (2022) 131930

Contents lists available at ScienceDirect

Chemosphere

journal homepage: www.elsevier.com/locate/chemosphere

Delineation of the exposure-response causality chain of chronic copper toxicity to the zebra mussel, *Dreissena polymorpha*, with a TK-TD model based on concepts of biotic ligand model and subcellular metal partitioning model

T.T. Yen Le [a,*], Nachev Milen [a], Daniel Grabner [a], A. Jan Hendriks [b], Willie J.G. M. Peijnenburg [c,d], Bernd Sures [a]

[a] Department of Aquatic Ecology and Centre for Water and Environmental Research (ZWU), Faculty of Biology, University of Duisburg-Essen, D-45141, Essen, Germany
[b] Department of Environmental Science, Faculty of Science, Radboud University Nijmegen, 6525, HP Nijmegen, the Netherlands
[c] Center for Safety of Substances and Products, National Institute for Public Health and the Environment, Bilthoven, 3720, BA, the Netherlands
[d] Institute for Environmental Sciences, Leiden University, 2311 EZ, Leiden, the Netherlands

HIGHLIGHTS

- A TK-TD model was constructed for delineating the exposure-response causality chain.
- Uptake was simulated considering water chemistry and biotic ligand characteristics.
- Potentially toxic pool was modelled based on metabolism, detoxification, elimination.
- Biomarker responses were related to the concentration of potentially toxic metal.

GRAPHICAL ABSTRACT

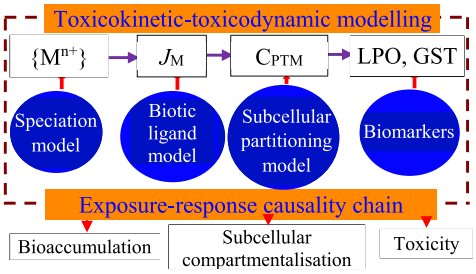

ARTICLE INFO

Handling Editor: James Lazorchak

Keywords:
Toxicokinetic-toxicodynamic model
Biotic ligand model
Subcellular partitioning
Chronic toxicity
Bivalves
Biomarkers

ABSTRACT

A toxicokinetic-toxicodynamic model was constructed to delineate the exposure–response causality. The model could be used: to predict metal accumulation considering the influence of water chemistry and biotic ligand characteristics; to simulate the dynamics of subcellular partitioning considering metabolism, detoxification, and elimination; and to predict chronic toxicity as represented by biomarker responses from the concentration of metals in the fraction of potentially toxic metal. The model was calibrated with data generated from an experiment in which the Zebra mussel *Dreissena polymorpha* was exposed to Cu at nominal concentrations of 25 and 50 μg/L and with varied Na^+ concentrations in water up to 4.0 mmol/L for 24 days. Data used in the calibration included physicochemical conditions of the exposure environment, Cu concentrations in subcellular fractions, and oxidative stress-induced responses, i.e. glutathione-S-transferase activity and lipid peroxidation. The model explained the dynamics of subcellular Cu partitioning and the effect mechanism reasonably well. With a low affinity constant for Na^+ binding to Cu^{2+} uptake sites, Na^+ had limited influence on Cu^{2+} uptake at low Na^+ concentrations in water. Copper was taken up into the metabolically available pool (MAP) at a largely higher rate than into the cellular debris. Similar Cu concentrations were found in these two fractions at low exposure

* Corresponding author.
E-mail address: yen.le@uni-due.de (T.T.Y. Le).

https://doi.org/10.1016/j.chemosphere.2021.131930
Received 22 June 2021; Received in revised form 3 August 2021; Accepted 16 August 2021
Available online 18 August 2021

levels, which could be attributed to sequestration pathways (metabolism, detoxification, and elimination) in the MAP. However, such sequestration was inefficient as shown by similar Cu concentrations in detoxified fractions with increasing exposure level accompanied by the increasing Cu concentration in the MAP.

1. Introduction

The response of aquatic organisms to metal exposure occurs as a causal consequence of a number of factors, from environmental availability, uptake, elimination to internal detoxification. Therefore, delineating the chain of exposure-response causality requires consideration of all these factors. Accordingly, extensive efforts have been put in taking take these factors into account, contributing to significant progress in environmental risk assessment for metals. One example is the development of speciation models for simulating metal bioavailability. Only the bioavailable fraction of the total amount of metals in the environment can be taken up by organisms (Peijnenburg et al., 2002). A significant fraction of the total metal is non-available due to formation of organic and inorganic metal complexes (Di Toro et al., 2001). Metal bioavailability depends on environmental chemistry, such as the concentrations of dissolved organic carbon (DOC), Na^+, and Ca^{2+} (Sprague, 1968; Pagenkopf et al., 1974; Allen et al., 1980; Playle, 1998). The proportion of various metal species could be predicted well by speciation models, e.g. WHAM (Tipping, 1998) and visual MINTEQ (Gustafson, 2011). Accordingly, the free metal ion activity model (FIAM) has been developed in which the free metal ions in solution are assumed to represent bioavailable metal species, determining metal uptake and subsequent toxicity (Morel, 1983; Campbell, 1995).

However, metal toxicity is not determined by the free metal ion activity alone (De Schamphelaere and Janssen, 2002; He et al., 2014). Protons (H^+) and other major cations (e.g. Na^+, Ca^{2+}, Mg^{2+}, K^+) might compete with metal ions at sites of toxic action (Playle et al., 1993; Playle, 1998), affecting metal toxicity (De Schamphelaere et al., 2005; Le et al., 2012). Both chemical speciation and cation competition are included in the biotic ligand model (BLM; Di Toro et al., 2001). This model assumes that metal toxicity results from the binding of free metal ions or other reactive species to physiologically active or transport sites at biotic ligands on the organism-water interface (Di Toro et al., 2001; De Schamphelaere and Janssen, 2002; Paquin et al., 2002). In the BLM, the hypothetical biotic ligand is usually the surface membrane, while only metals internalised into the cells can initiate effects (Croteau and Luoma, 2009). In addition, metal concentrations at target sites are hardly quantified for invertebrates. Despite that, the BLM principle can be applied to estimate the uptake rate considering cation competition (Slaveykova and Wilkinson, 2005; Wang and Tan, 2019).

The approach mentioned above as well as other biokinetic models can estimate metal uptake and the internal concentration reasonably well. However, adverse effects might not be directly related to the total body burden because of the sequestration of internalised metals by subcellular ligands and its role in the tolerance to metal exposure (Rainbow, 2002, 2007; Vijver et al., 2004; de Paiva Magalhaes et al., 2015). The association of metals with insoluble metal-rich granules (MRG) or the binding to heat-stable proteins in the cytosol (or metallothionein-like proteins, MTLP) reflects the detoxification capacity (Wallace et al., 2003; Vijver et al., 2004; Rainbow et al., 2011). By

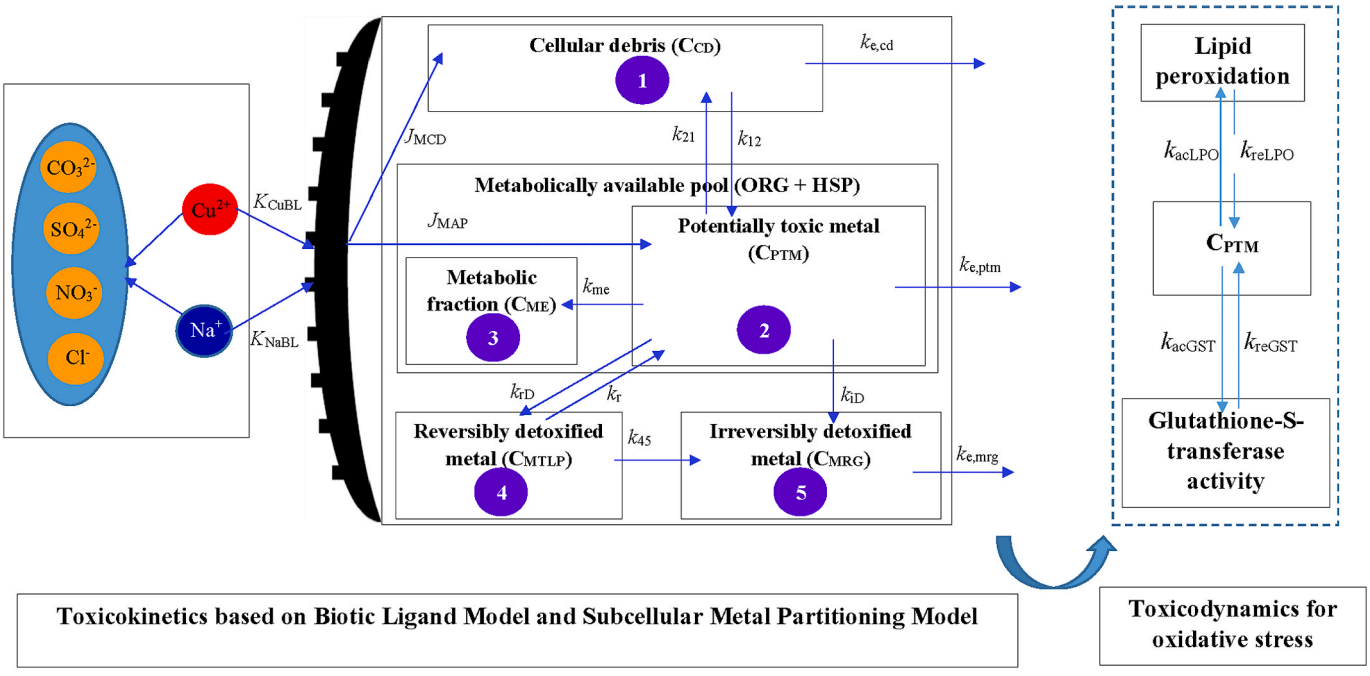

Fig. 1. A toxicokinetic-toxicodynamic (TK-TD) model with the accumulation of metals in the potentially toxic metal fraction (C_{PTM}) as the connecting point. Simulation of the TK phase is based on the concepts of the biotic ligand model, i.e. the metal uptake rate depends on the activity of free metal ions (speciation model) and the interactions of free metal ions with the biotic ligands at the gills (represented by the binding constants K_{CuBL} and K_{NaBL}); and the subcellular metal partitioning model: metals taken up via gills are distributed to the metabolically available pool (including metals in association with organelles ORG and head-sensitive proteins HSP) and the cellular debris with the rates J_{MAP} and J_{CD}, respectively. Metals can be transported between these two fractions with rates k_{12} and k_{21}. From the cellular debris, metals can be eliminated at a rate constant $k_{e,cd}$. Part of the metal in the MAP is used in the metabolic processes (C_{ME}), while the excess metal above the metabolic requirement is built-up in the potentially toxic metal pool (C_{PTM}) where metals can be reversibly detoxified by binding to metallothionein-like proteins with a detoxification rate constant k_{rD} (C_{MTLP}), irreversibly detoxified by the storage in metal-rich granules (C_{MRG}) with a detoxification rate constant k_{iD}, or eliminated at a rate constant $k_{e,ptm}$. Part of reversibly detoxified metals can be released back to the MAP, which can be used in metabolism, or internalised into the metal-rich granules with a rate constant k_{45}. Part of irreversibly detoxified metals can be eliminated at a rate constant $k_{e,mrg}$.

contrast, interactions of metals with physiologically sensitive molecules (e.g. small peptides, heat-sensitive proteins, DNA and RNA) or organelles (mitochondria, nuclei, and membranes) account for potential interference of metals on essential physiological processes (Serafim and Bebianno, 2007; Pan and Wang, 2008; Blanchard et al., 2009; Kamunde, 2009). Although metal concentrations in various subcellular fractions could be experimentally quantified by standardized biochemical fractionation techniques (Wallace et al., 1998, 2003, 2003; Blackmore and Wang, 2002), subcellular metal partitioning is a dynamic process (Wang and Rainbow, 2006; Campana et al., 2015), requiring modelling approaches for a mechanistic understanding.

Toxicokinetic-toxicodynamic (TK-TD) models simulate the time-course processes that determine adverse effects on organisms (Ashauer and Escher, 2010; Jager et al., 2011). With evident advantages, these models have been widely applied for predicting acute toxicity (Gao et al., 2015, 2017; Feng et al., 2018), and only recently for chronic toxicity (Le et al., 2021a). In most of the previous TK-TD models, the total internal concentration was considered the connecting point between the TK phase and the TD phase. In the former, the internal concentration was usually predicted from the total or dissolved metal concentration in the solution, ignoring potential influence of water chemistry on chemical speciation or on metal uptake (Jager et al., 2011; Tan and Wang, 2012; Ashauer et al., 2013). In the later, acute toxicity is usually related to the internal metal concentration (e.g. Ashauer et al., 2013; Gao et al., 2015; Feng et al., 2018), excluding the significance of internal metal sequestration.

Considering the importance of the above issues, the influence of water chemistry has been considered in some recently developed TK-TD models (Gao et al., 2015, 2017, 2017; Feng et al., 2018), while subcellular metal partitioning has been integrated in some others (Tan and Wang, 2012). However, a TK-TD model in which all the factors are simultaneously considered in modelling the response of organisms to metal exposure is still not available, preventing a delineation of the whole exposure-response causality. Therefore, the aim of the present study is to develop a TK-TD model for delineating the exposure-response causality chain determining chronic Cu toxicity to the Zebra mussel by including: 1) water chemistry in simulating metal uptake; 2) subcellular metal partitioning in predicting the concentration of potentially toxic metal; and 3) biomarker responses at sub-lethal levels.

2. Materials and methods

2.1. Model specification

The TK-TD model developed in the present study delineates and links the processes involved in the exposure-response causality chain: bioavailability influenced by water chemistry; uptake as a function of water properties and biotic ligand characteristics; subcellular metal partitioning as a result of metabolism, detoxification, and elimination; and physiological responses of organisms determined by the fraction of potentially toxic metal (Fig. 1). In the TK phase, metal uptake was simulated based on the BLM concept to account for the effects of chemical speciation and cation competition. Subsequently, metals are taken up to the cellular debris and the metabolically available pool (MAP; consisting of metals in association with organelles ORG or heat-sensitive proteins HSP) (Fig. 1). In addition, the concentration in the fraction of potentially toxic metal was simulated considering various chelation pathways. Excess metals in the MAP (i.e. above the metabolic requirements in combination with the detoxification and elimination capacity) form the fraction of potentially toxic metal (PTM) as a balance of uptake, metabolism, elimination, and detoxification (Fig. 1). This compartment was assumed to represent the fraction of metals at sites of toxic action. On the one hand, this approach is in accordance with the previous findings that sub-lethal effects of Cu were related to the build-up of Cu in non-detoxified pools (Rainbow and Smith, 2013; Kalman et al., 2015). On the other hand, the proposed approach allows for distinguishing the metal required for metabolic processes from the metabolically available species. In the TD phase, biological responses were linked to the concentration of potentially toxic metal.

2.2. Model characterisation

2.2.1. Toxicokinetic simulation

Metals as free ions are taken up to the cellular debris (Compartment 1) and the MAP (Fig. 1; Wang, 2013). In the cellular debris, metal accumulation depends on the uptake of free ions from the dissolved phase (J_{CD}; μg/g/d), elimination ($k_{e,CD}$; 1/d), and the transport to and from the MAP (k_{12} and k_{21}; 1/d, respectively) (Fig. 1). Waterborne metals are transported from the MAP to the detoxified pools (Ng and Wang, 2005). Accordingly, detoxified and metabolically available pools are distinguished (Vijver et al., 2004; Luoma and Rainbow, 2008; Rainbow and Luoma, 2011b). In the MAP, metals are used for essential metabolic processes (represented by the metabolic fraction as compartment 2; C_{ME}) at a rate constant k_{me} (1/d), while the excess metal forms the fraction of potentially toxic metal (C_{PTM}; compartment 3). Excess metals can be eliminated with a rate constant $k_{e,PTM}$ (1/d), reversibly detoxified by binding to MTLP at a rate constant k_{rD} (1/d) (forming the reversibly detoxified or MTLP fraction C_{MTLP}; compartment 4), or irreversibly detoxified via incorporation into the MRG with a rate constant k_{iD} (1/d) (forming the irreversibly detoxified or MRG fraction C_{MRG}; compartment 5). The MTLP and MRG fractions constitute the biologically detoxified metal (BDM). Furthermore, reversibly detoxified metals can be released from binding to MTLP back to the MAP (k_r; 1/d) where they can be used in metabolism (Brouwer et al., 2002; Amiard et al., 2006). Irreversibly detoxified metals can be excreted due to the elimination of the granules ($k_{e,MRG}$; 1/d) (Gibbs et al., 1998; Vijver et al., 2004). Moreover, reversibly detoxified metals can be incorporated into the MRG due to the breakdown of a lysosome (represented by a rate constant k_{45}) (Luoma and Rainbow, 2008). The above simulation accounts for the elimination from both the excess fraction and from the detoxified fraction, which has been reported for essential metals (Rainbow, 2002). Metal accumulation in the PTM fraction occurs as a function of uptake, metabolism, detoxification, and elimination (Fig. 1). Consequently, the internal metal concentration can be written as:

$$C_{int} = C_{CD} + C_{ME} + C_{PTM} + C_{MTLP} + C_{MRG} \quad (1)$$

According to the BLM concept, cations like Na^+ might form complexes with biotic ligands at a ratio expressed by an affinity constant, assuming that the complexation capacity is independent of water quality (De Schamphelaere and Janssen, 2002). In the presence of Na^+, Cu^{2+} uptake (J_{Cu}; μg/g/d) can be described by a competitive saturation equation as written by Sunda and Huntsman (1998):

$$J_{Cu} = \frac{J_{max} \times \{Cu^{2+}\} \times K_{CuBL}}{\{Cu^{2+}\} \times K_{CuBL} + \{Na^{+}\} \times K_{NaBL} + 1} \quad (2)$$

where J_{max} (μg/g/d) is the maximum uptake rate obtained at saturation of the transport sites; $\{Cu^{2+}\}$ and $\{Na^{+}\}$ (mol/L) are free ion activities of Cu^{2+} and Na^{+} in water; K_{CuBL} and K_{NaBL} (L/mol) are affinity constants for the binding of Cu^{2+} and Na^{+} to the Cu^{2+} transport site, respectively. A similar approach has been applied for simulating metal accumulation in recently developed TK-TD models (Gao et al., 2015, 2017; Feng et al., 2018; Wang and Tan, 2019). In this equation, the maximum uptake rate and the affinity constants can be determined by fitting the data on metal accumulation (Gao et al., 2015).

Taking all these processes into consideration, the metal concentration in the cellular debris could be expressed as a function of the uptake of free metal ions (the 1st factor), elimination (the 2nd factor), and the transport with the MAP (last factors):

$$\frac{dC_{CD}}{dt} = \frac{J_{maxCD} \times K_{CuBL} \times \{Cu^{2+}\}}{1 + K_{CuBL} \times \{Cu^{2+}\} + K_{NaBL} \times \{Na^{+}\}} - k_{e,CD} \times C_{CD} + (k_{21} \times C_{PTM} - k_{12} \times C_{CD}) \quad (3)$$

where C_{CD} (μg/g dw) is the Cu concentration in the cellular debris; J_{maxCD} (μg/g dw/d) is the maximum Cu^{2+} influx rate to the cellular debris; K_{CuBL} and K_{NaBL} (L/mol) are the affinity constants of Cu^{2+} and Na^{+} to Cu^{2+} uptake sites, respectively; $\{Cu^{2+}\}$ and $\{Na^{+}\}$ (mol/L) are the free ion activities of Cu^{2+} and Na^{+} in the external medium, respectively; $k_{e,CD}$ (1/d) is the rate constant for Cu elimination from the cellular debris; and k_{12} and k_{21} (1/d) represent the Cu transport between the cellular debris and the MAP (Wang, 2013).

Similarly, metal accumulation in the PTM is a function of the uptake of free metal ions from the solution (the 1st factor), the exchange with the cellular debris (the 2nd factor), the release of reversibly detoxified metals from binding to MTLP (the 3rd factor), metabolism (the 4th factor), and detoxification and elimination (last factors):

$$\frac{dC_{PTM}}{dt} = \frac{J_{maxMAP} \times K_{CuBL} \times \{Cu^{2+}\}}{1 + K_{CuBL} \times \{Cu^{2+}\} + K_{NaBL} \times \{Na^{+}\}} + (k_{12} \times C_{CD} - k_{21} \times C_{PTM}) + k_r \times C_{MTLP} - \frac{dC_{ME}}{dt} - (k_{rD} + k_{iD} + k_{e,PTM}) \times C_{PTM} \quad (4)$$

with k_r (1/d) being the rate constant at which reversibly detoxified metals are released back to the MAP. This equation reflects the dependence of the build-up of excess metals on uptake, metabolism, detoxification, and elimination. The concentration of metals in the metabolic fraction (C_{ME}; μg/g) was modelled as a function of the metabolic requirement, which acts as the maximum concentration in this fraction, as applied by Veltman et al. (2014) for modelling Na^{+} influx and by Le et al. (2021a) for modelling the binding of Na^{+} to Na^{+}/K^{+}-ATPase enzymes:

$$\frac{dC_{ME}}{dt} = k_{me} \times C_{PTM} \times \left(1 - \frac{C_{ME}}{Me_{max}}\right) \quad (5)$$

with k_{me} (1/d) being the metabolism rate constant; and Me_{max} (μg/g dw) representing the maximum metabolic requirement. The maximum metabolic requirement is indicative of the maximum concentration of Cu used in metabolic processes. The Cu concentration in the MAP measured in the mussels living in a Cu-depleted environment cannot appropriately reflect this parameter. Instead, it was parameterised based on theoretical estimates of metabolic requirements derived by White and Rainbow (1985). Requirements for enzymes and for respiratory pigment proteins were considered in the estimation (White and Rainbow, 1985). In this approach, enzyme requirements were theoretically estimated from the number of copper-bearing enzymes and their proportions in the total number of enzymes in metabolizing tissues (White and Rainbow, 1985). Within the bivalvia, hemocyanins are restricted to the Protobranchia (Markl, 2013). Markl (private communication) suggested that the ancestors of other bivalves lost hemocyanins during evolution to adapt to their sessile filter-feeding lifestyle. Accordingly, hemocyanins were not included in the theoretical estimate of Cu metabolic requirements in the Zebra mussel. An estimate of the enzyme requirement of 26.3 μg/g dw (excluding haemocyanins) obtained by White and Rainbow (1985) was deployed to represent the maximum metabolic requirements for Cu.

Replacing Equation (5) to Equation (4) results in

$$\frac{dC_{PTM}}{dt} = \frac{J_{maxMAP} \times K_{CuBL} \times \{Cu^{2+}\}}{1 + K_{CuBL} \times \{Cu^{2+}\} + K_{NaBL} \times \{Na^{+}\}} + (k_{12} \times C_{CD} - k_{21} \times C_{PTM}) + k_r \times C_{MTLP} - k_{me} \times C_{PTM} \times \left(1 - \frac{C_{ME}}{Me_{max}}\right) - (k_{rD} + k_{iD} + k_{e,PTM}) \times C_{PTM} \quad (6)$$

Combining Equations (5) and (6) provides an estimation of the metal concentration in the MAP:

$$\frac{dC_{MAP}}{dt} = \frac{J_{maxMAP} \times K_{CuBL} \times \{Cu^{2+}\}}{1 + K_{CuBL} \times \{Cu^{2+}\} + K_{NaBL} \times \{Na^{+}\}} + (k_{12} \times C_{CD} - k_{21} \times C_{PTM}) + k_r \times C_{MTLP} - (k_{rD} + k_{iD} + k_{e,PTM}) \times C_{PTM} \quad (7)$$

Similar mass-balance equations were used to describe metal concentrations in the reversibly (C_{MTLP}; μg/g dw) and irreversibly (C_{MRG}; μg/g dw) detoxified fractions:

$$\frac{dC_{MTLP}}{dt} = k_{rD} \times C_{PTM} - k_{45} \times C_{MTLP} - k_r \times C_{MTLP} \quad (8)$$

$$\frac{dC_{MRG}}{dt} = k_{iD} \times C_{PTM} + k_{45} \times C_{MTLP} - k_{e,MRG} \times C_{MRG} \quad (9)$$

with k_{rD} (1/d) and k_{iD} (1/d) being detoxification rate constants; and k_{45} (1/d) being the rate constant at which reversibly detoxified metals are agglomerated into the MRG.

Therefore, the total internal Cu concentration (C_{int}; μg/g dw) can be expressed as:

$$\frac{dC_{int}}{dt} = \frac{(J_{maxCD} + J_{maxMAP}) \times K_{CuBL} \times \{Cu^{2+}\}}{1 + K_{CuBL} \times \{Cu^{2+}\} + K_{NaBL} \times \{Na^{+}\}} - k_{e,CD} \times C_{CD} - k_{e,PTM} \times C_{PTM} - k_{e,MRG} \times C_{MRG} \quad (10)$$

This equation was a modified version from those developed by Gao et al. (2015, 2017) and Feng et al. (2018) so that metal elimination was specified from the cellular debris, PTM, and MRG fractions (Wang, 2013).

2.2.2. Toxicodynamic simulation

In acute TK-TD models, a lower threshold level is usually included in the ordinary differential equation relating adverse effects to the internal metal concentration or the metal concentration at the target site (Jager et al., 2011; Ashauer et al., 2013; Gao et al., 2015, 2017; Wang and Tan, 2019). In chronic exposure at sub-lethal levels, biomarker responses have been observed even at the background concentration (See discussion). Therefore, such a threshold was not included. By contrast, a recovery rate constant was integrated to account for recovery processes, e.g. repair mechanisms at cellular levels and physiological adaptation (Ashauer et al., 2007; Jager et al., 2011). As such, biological responses of organisms were expressed as:

$$\frac{dGST}{dt} = k_{acGST} \times C_{PTM} - k_{reGST} \times GST \quad (11)$$

$$\frac{dLPO}{dt} = k_{acLPO} \times C_{PTM} - k_{reLPO} \times LPO \quad (12)$$

where k_{acGST} and k_{acLPO} (units of GST or LPO/(μmol/g dw)/d) are the rate constants for damage accrual; and k_{reGST} and k_{reLPO} (1/d) regard the damage recovery.

All mathematical equations of the final model is given in SA, Supporting Information.

2.3. Identifiability and sensitivity analyses

A structural identifiability analysis was conducted using GenSSI2 (Chis et al., 2011; Ligon et al., 2018) to examine the possibility of the model to deliver a unique solution for the unknown parameters with noise-free data. The analysis demonstrated that the developed model was structurally identifiable with a number of parameters being globally identifiable. In addition, a sensitivity analysis was implemented using the MATLAB-based AMIGO toolbox (Balsa-Canto et al., 2010) to assess the global ranking of the unknown parameters regarding their influence on model estimation. This analysis is based on Latin hypercube sampling in which effects of changes in parameters on model outputs are

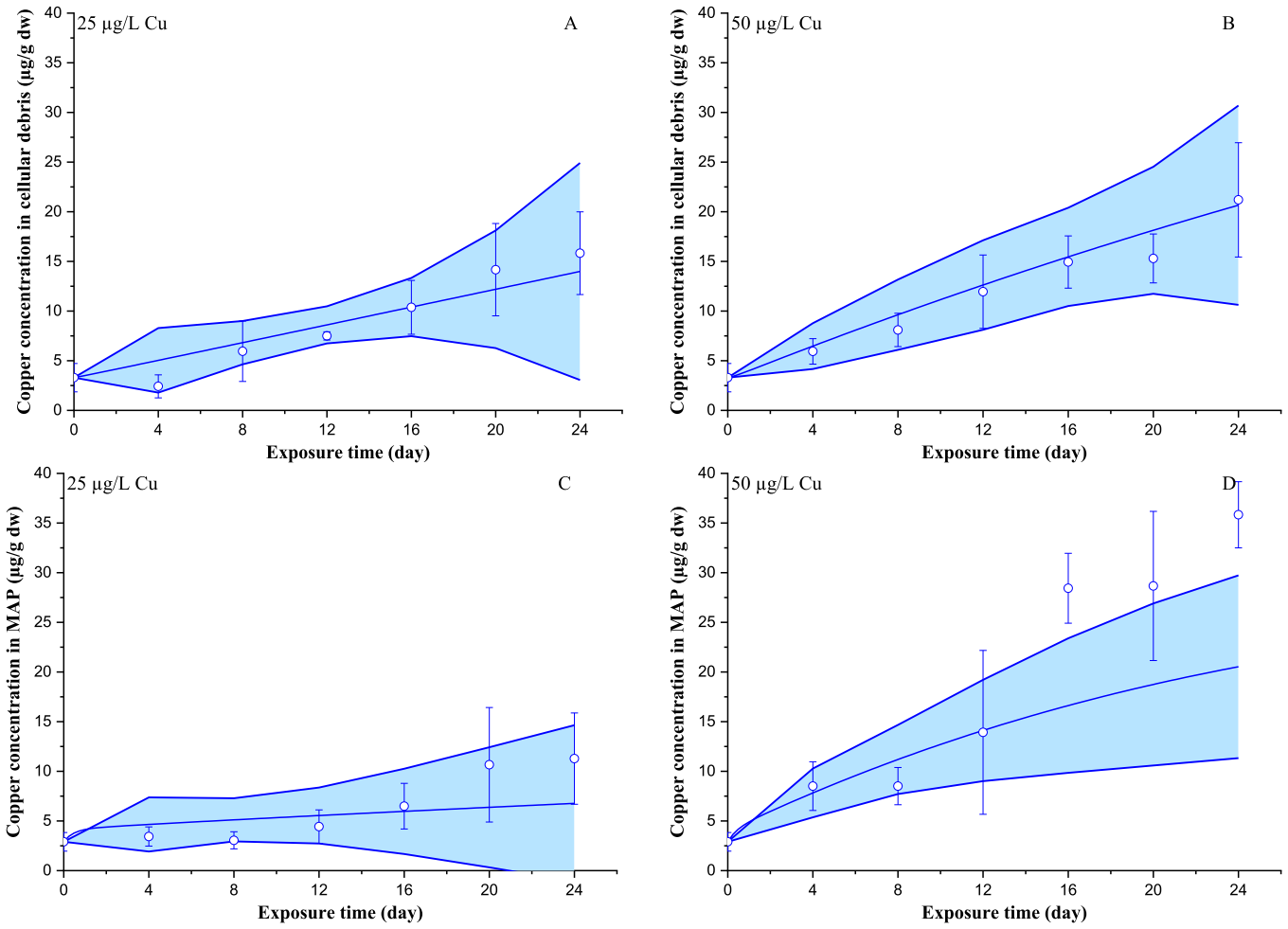

Fig. 2. The relationship between the measurements and the estimates of Cu concentrations in subcellular fractions: cellular debris (A and B), metabolically available pool (MAP; C and D), reversibly detoxified fraction in binding with metallothionein-like protein (MTLP; E and F), irreversibly detoxified fraction in association with metal-rich granules (MRG; G and H); and of biomarker responses in terms of glutathione-S-Transferase (GST) activity (I and J) and lipid peroxidation (LPO; K and L) at nominal concentrations of 25 (on the left site) and 50 µg/L Cu (on the right site). The areas covered by the solid lines represent the confidence interval with the line in the middle representing the mean estimate. Dots and bars represent the measurements (average ± standard deviation) when Na^+ was added to the reconstituted water at 0.5 mmol/L.

quantified considering interactions between parameters (Balsa-Canto et al., 2010). The analysis revealed that the model estimation was least sensitive to the rate constant for Cu elimination from the cellular debris ($k_{e,CD}$).

2.4. Model calibration

Unknown parameters were determined by fitting data to the final model (SA, supporting Information) using the MATLAB-based AMIGO toolbox (Balsa-Canto et al., 2016). Data required for model calibration included: 1) the free Cu^{2+} and Na^+ activities obtained from the speciation model as mentioned above; 2) Cu concentrations in the cellular debris, MRG, MTLP, and MAP fractions; and 3) lipid peroxidation (LPO) and the glutathione-S-transferase (GST) activity. Such data were obtained from an exposure experiment in which the Zebra mussel (*Dreissena polymorpha*) was exposed to waterborne Cu for 24 days at nominal concentrations of 25 and 50 µg/L when Na^+ was added to the reconstituted water at concentrations of 0.5, 1.5, 2.7, and 4.0 mmol/L (Le et al., 2021b). Water was renewed daily and sampled for measurements of dissolved metal concentration after water renewal and 24-h post water renewal (Le et al., 2021b). Mussels were sampled once in four days and stored at −80 °C for further analyses.

The analysis of metal concentrations in water was described in Le et al. (2021b). Daily concentrations were calculated as the mean of the initial and final metal concentrations for each renewal interval. The mean of these daily concentrations (Table S1, Supporting Information) was considered the actual exposure level for estimating free metal ion activities with the WHAM model (Tipping, 1998). The pH, the measured dissolved Cu concentration, and the water chemistry of the reconstituted water (Osterauer et al., 2010) were used as input parameters to achieve estimates of free metal ion activities of Cu and Na ({Cu^{2+}} and {Na^+}, respectively). Subsequently, the free metal ion activities were deployed as inputs for model calibration. The measurements of the biomarkers were described in Le et al. (2021a) with the raw data being given in the Supporting Information (Tables S6 and S7). A description of the investigation for subcellular Cu partitioning is shown below while the data on Cu concentrations in subcellular fractions are presented in Tables S2, S3, S4, and S5, Supporting Information.

In the model calibration, the affinity constants of Cu^{2+} and Na^+ for the copper uptake sites were assumed to be independent of water chemistry, following the assumption of the BLM (De Schamphelaere and Janssen, 2002). A similar assumption was applied for the maximum

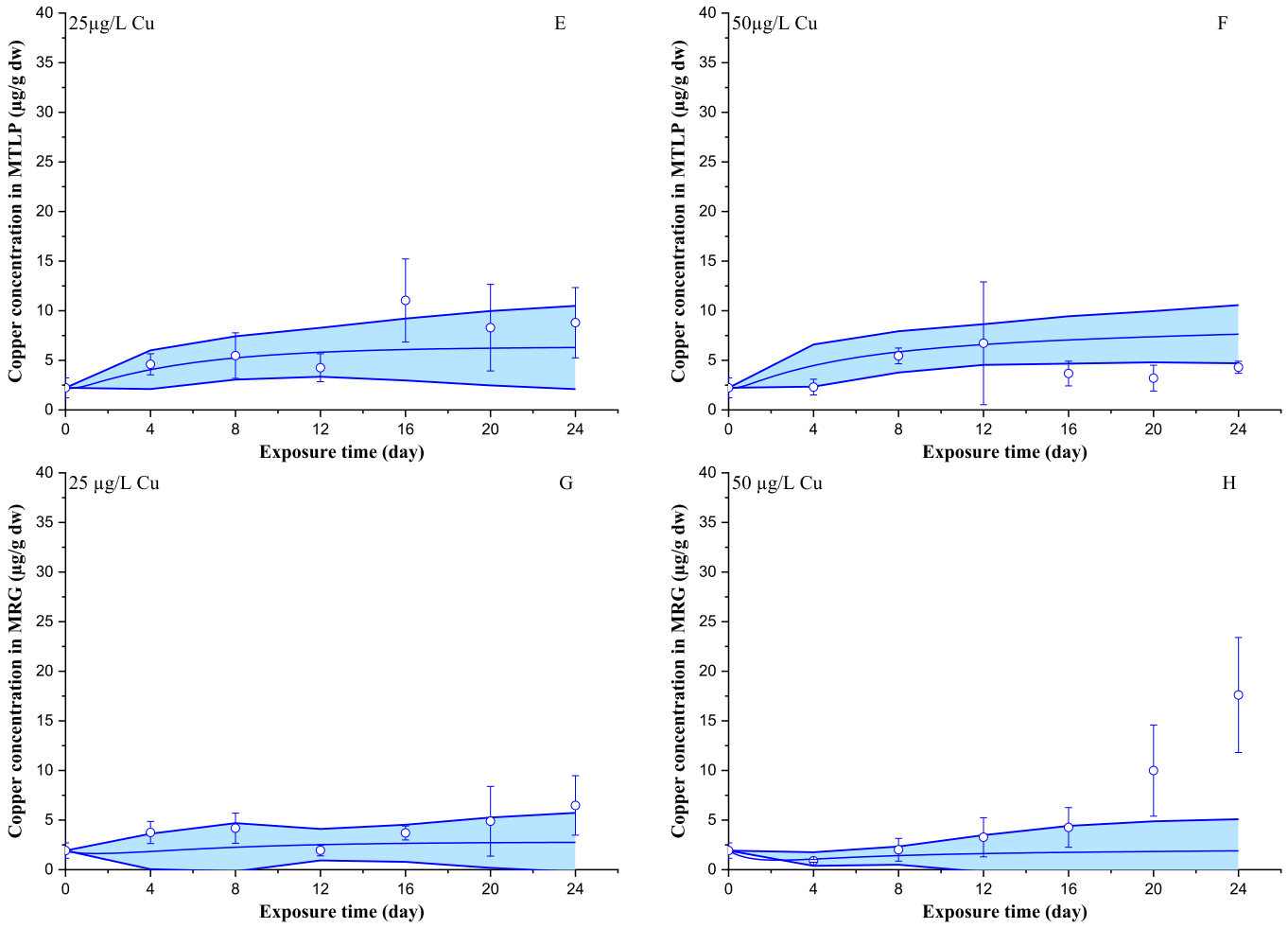

Fig. 2. (*continued*).

uptake rate as well as for the damage accrual and recovery rate constants. By contrast, the parameters determining subcellular metal partitioning was assumed to be influenced by the exposure level, not the Na^+ concentration in water. This assumption is based on negligible interactions between Cu and major cations in the intracellular trafficking and transport (Handy et al., 2002). Because of the least sensitivity of the model estimates to the rate constant that Cu was eliminated from the cellular debris ($k_{e,CD}$), this parameter was excluded from the model calibration.

2.5. Subcellular copper fractionation and metal analyses

The subcellular fractionation was conducted according to the widely applied approach developed by Wallace et al. (2003). After being removing from the shell, mussel soft tissue from two mussels was pooled together and homogenised in cold 20 mM TRIS buffer (pH 7.6) at a ratio of 1: 10 w/v using an UltraTurrax tissue homogeniser. The homogenate was then centrifuged at 1,450×*g* and 4 °C for 15 min. The pellet was digested in 1 M NaOH at 90–95 °C for 10 min in a water bath. The mixture was then centrifuged at 5,000×*g* for 10 min to separate the cellular debris in the supernatant from MRG as pellets. The supernatant from the 1,450×*g* centrifugation was centrifuged at 100,000×*g* for 1 h to separate the organelle fraction in the pellet from the cytosol in the supernatant. The supernatant was heated at 80 °C in a water bath for 10 min, cooled for 1 h in ice, and subsequently centrifuged at 30,000×*g* and 4 °C for 30 min to separate HSP (mainly enzymes) in the pellet and MTLP in the supernatant. Four replicates (8 individuals) were implemented for each sample. Procedural blanks, i.e. without tissues, were processed with the same protocol to take the correction for laboratory and equipment contamination. Each fraction was dried at 105 °C and digested with 4 mL HNO_3 (65%, sub-boiled) using a MARS 6 microwave digestion system (CEM GmbH, Kamp-Lintfort, Germany; Le et al., 2021b). Concentrations of Cu in the digested samples as well as in water samples were analysed using a Perkin-Elmer-Sciex DCR-e inductively coupled plasma mass spectrometer as described in our previous study (Le et al., 2021b). The concentration of Cu in the MAP was derived from the concentrations in the organelle and HSP fractions.

3. Results and discussions

In general, the TK-TD model developed was able to capture variations in both Cu concentrations in subcellular fractions and oxidative stress-caused responses in the Zebra mussel (Fig. 2 and Figs. S1, S2, S3). Estimates (mean ± error bound margin) for unknown parameters of the TK-TD model determined in model calibration are given in Table 1. By integrating the influence of exposure conditions (in both terms of metal availability and cation competition) and biotic ligand characteristics on metal uptake, the influence of metabolism as well as the detoxification and elimination capacity, the model allows for delineating the exposure-response causality chain.

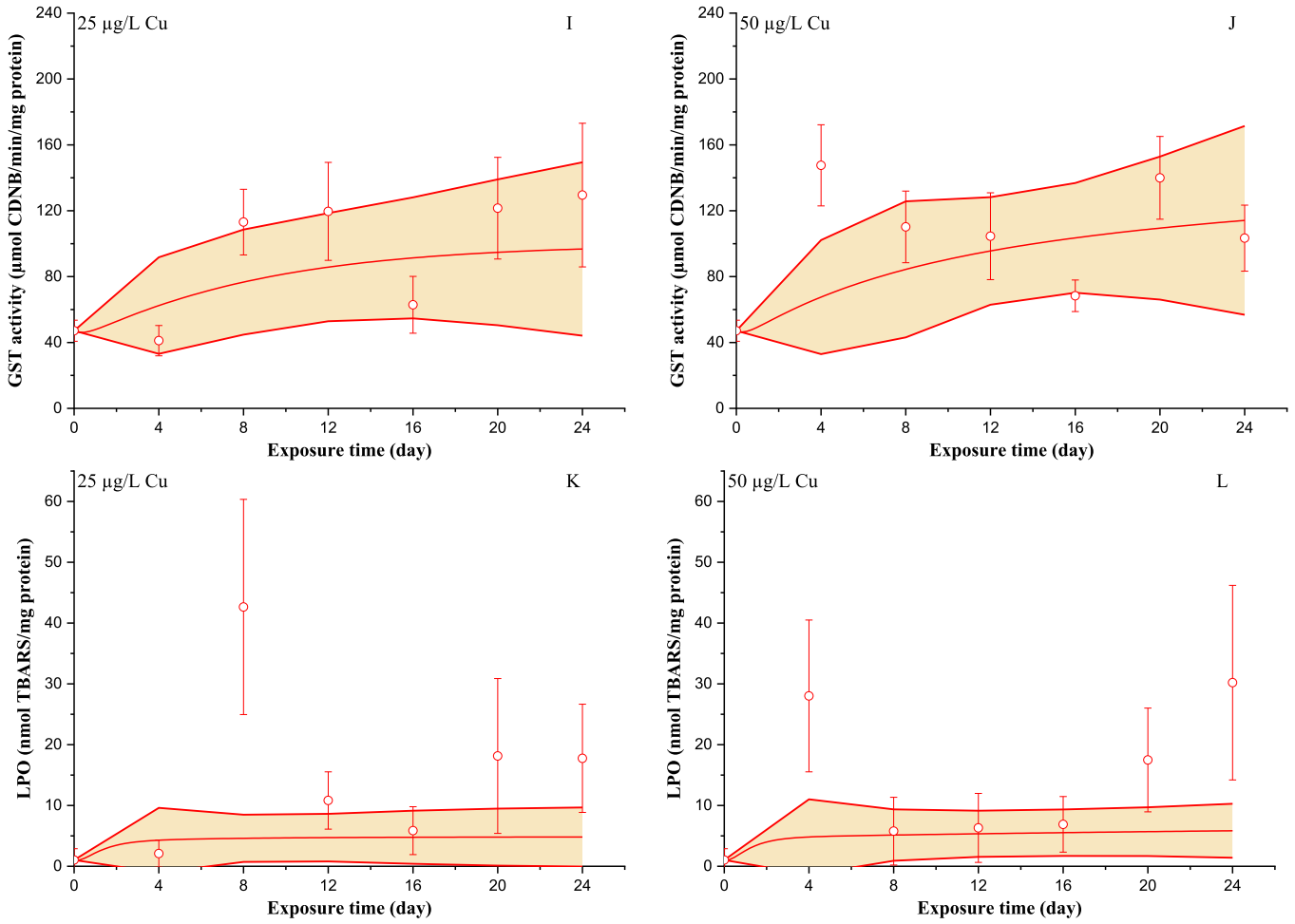

Fig. 2. (*continued*).

3.1. *Influence of water chemistry on metal uptake and the BLM-aided toxicokinetic modelling*

With the chemical properties of organic matter-free reconstituted water, the Na^+ concentration in water hardly affected Cu speciation and bioavailability. This was displayed by limited changes in the free copper ion activity with changed Na^+ concentration from 0.5 to 4.0 mmol/L generated by the chemical speciation with the WHAM VII model. The affinity constant for Na^+ binding to Cu^{2+} uptake sites was substantially lower than that for Cu^{2+} (Table 1). According to Gao et al. (2015), the BLM-aided approach as applied in the present study allows for considering the impacts of species characteristics (represented by the biotic ligand) and water chemistry on metal uptake. The low affinity constant of Na^+ for Cu^{2+} uptake sites contributed to limited influence of Na^+ on Cu uptake by the Zebra mussel at low Na^+ concentrations in water (Fig. 2 and Figs. S1, S2, S3). However, it is not indicative of a lack of a competition between Na^+ and Cu^{2+}. The affinity constant is a ratio of the kinetic rate constant for the complexation with the membrane transport site to a combination of the constant for dissociation of metals back to the medium and the constant for the internalisation of the metal across the membrane into the cytoplasm (Sunda and Huntsman, 1998). The affinity constant for Na^+ binding to Cu^{2+} uptake sites is substantially lower than the affinity constant for binding to sites of toxic action derived by the BLM (Niyogi and Wood, 2004). By contrast, the affinity constant for Cu^{2+} binding to the uptake sites in the present study was similar to that of Cu^{2+} binding to sites of toxic action determined by the BLM (Niyogi and Wood, 2004). According to Feng et al. (2018), similar affinity constants, which were derived based on accumulation and toxicity data, correspond to the case that both the sites of uptake and the sites of toxic action are on the membrane surface in organisms. Alternatively, different values of affinity constant reflect the differences between the location of uptake sites and sites of toxic action, i.e. the former on the surface of the cell membrane while the later inside the cell.

3.2. *Subcellular metal partitioning and the fraction of potentially toxic metal*

Copper was taken up to the MAP at a substantially higher rate than to the cellular debris ($J_{maxCD} \ll J_{maxMAP}$; Table 1). However, such a gap was not seen in Cu concentrations in these two pools (Fig. 2A-B-C-D and Figs. S1A-B-C-D, S2A-B-C-D, S3A-B-C-D), attributed to the difference in sequestration strategies exhibited by model calibration results (Table 1). The concentration of Cu in the cellular debris was negligibly affected by outfluxes (elimination and transport to the MAP) compared to the influxes (uptake from solution and transport from the MAP) as shown in Table 1, contributing to steady increases in the Cu concentration in this compartment (Fig. 2A–B and Figs. S1A-B, S2A-B, S3A-B). By contrast, the Cu concentration in the MAP was influenced by various outfluxes (i.e. transport to the cellular debris, elimination, and detoxification; Table 1). At a nominal concentration of 25 µg/L, similar concentrations of Cu in these two fractions (Fig. 2A–C and Figs. S1A-C, S2A-C, S3A-C) reflected the ability of the Zebra mussel to detoxify and eliminate Cu in the MAP (Table 1). However, such an observation was not seen at the higher exposure level (Fig. 2B–D and Figs. S1B-D, S2B-D, S3B-D), indicating the spill-over of these sequestration pathways.

Model calibration results showed the dependence of other kinetic

Table 1
Estimates (±error bound margin) for unknown parameters of the TK-TD model simulating chronic Cu toxicity at two exposure concentrations.

Symbol	Parameter	Unit	25 μg/L Cu	50 μg/L Cu
J_{maxCD}	Maximum Cu uptake rate to the cellular debris	μg/g/d	0.89 (±8.12)	
J_{maxMAP}	Maximum Cu uptake rate to the metabolically available pool	μg/g/d	6.20 (±45)	
$LogK_{CuBL}$	The affinity constant for the binding of Cu^{2+} to the Cu binding sites (in logarithm)	L/mol	8.57 (±5.91)	
$LogK_{NaBL}$	The affinity constant for the binding of Na^{+} to the Cu binding sites (in logarithm)	L/mol	−2.79 (±89)	
k_{12}	The rate constant for Cu transport from the cellular debris to the metabolically available pool	1/d	$9.40 \cdot 10^{-5}$ (±0.09)	0.02 (±0.11)
k_{21}	The rate constant for Cu transport from the metabolically available pool to the cellular debris	1/d	0.04 (±2.16)	0.25 (±2.82)
k_r	The rate constant for Cu release from the binding with MTLP to the metabolically available fraction	1/d	0.10 (±1.12)	0.01 (±1.20)
k_{rD}	The reversible detoxification rate constant	1/d	0.97 (±1.28)	0.92 (±0.95)
k_{iD}	The irreversible detoxification rate constant	1/d	0.33 (±1.92)	0.10 (±1.44)
k_{45}	The rate constant for incorporation of MTLP-bound Cu into the MRG	1/d	0.13 (±0.81)	0.21 (±1.05)
$k_{e,PTM}$	The rate constant for Cu elimination from the potentially toxic metal pool	1/d	0.80 (±8.47)	0.80 (±11)
k_{me}	The metabolism rate constant	1/d	0.08 (±0.24)	0.73 (±1.03)
$k_{e,MRG}$	The rate constant for Cu elimination from the MRG	1/d	0.48 (±2.70)	0.92 (±5.70)
k_{acGST}	The damage accurate constant for GST activity	Unit of GST/(μg/g)/d	9.75 (±14)	
k_{reGST}	The damage recovery constant for GST activity	1/d	0.15 (±0.34)	
k_{acLPO}	The damage accurate constant for LPO	Unit of LPO/(μg/g)/d	3.47 (±27)	
k_{reLPO}	The damage recovery constant for LPO	1/d	1.10 (±9.29)	

parameters on the exposure level (Table 1). For example, the Cu transport between the cellular debris and the MAP (represented by k_{12} and k_{21}) was increased with increasing Cu exposure level (Table 1). At the low exposure level, Cu was released from the binding to MTLP back to the MAP (k_r) at a high rate to fulfill Cu requirement for metabolic processes (Table 1). By contrast, this flow was negligible at the higher exposure level as the concentration of Cu in the MAP exceeded the metabolic requirements (Table 1). Both the detoxification by binding to MTLP and elimination from the MAP decreased with increasing exposure level (Table 1), implying spill-over effects of the detoxification mechanisms. Contrasting with such a trend for Cu accumulation in the MAP, Cu was eliminated from the MRG at a higher rate at an exposure level of 50 μg/L compared to 25 μg/L (Table 1). Additionally, Cu was used for metabolic processes at an increasing rate with increasing exposure level (Table 1). Such changes demonstrated the dynamics in subcellular Cu compartmentalisation.

The model also unraveled the differences between two detoxification pathways (Table 1). Copper binding to MTLP (reversible detoxification) occurred at a higher rate than the incorporation into the MRG (irreversible detoxification) ($k_{rD} \gg k_{iD}$; Table 1). This trend might explain higher concentrations of Cu bound to MTLP than the concentrations in the MRG (Fig. 2E-F-G-H; and Figs. S1E-F-G-H, S2E-F-G-H, S3E-F-G-H). The distribution of Cu to these two fractions additionally depended on the incorporation of MTLP-bound Cu into the MRG as well as the elimination from the MRG, which both increased with exposure concentration (Table 1). A higher rate of reversible detoxification compared to a combination of the rates for Cu dissociation from the binding to MTLP and for incorporation into the MRG (Table 1) resulted in slight increases in the Cu concentration in the MTLP fraction (Fig. 2E–F and Figs S1E-F, S2E-F, S3E-F). In addition to the elimination, the lower irreversible detoxification as well as the low incorporation of MTLP-bound Cu to the MRG contributed to the stability of Cu concentrations in the MRG during the 24-day exposure (Fig. 2G–H and Figs. S1G-H, S2G-H, S3G-H).

In comparison to the predictions of Cu concentrations in the cellular debris, MAP, and MTLP fractions, the estimates of Cu concentrations in the MRG deviated more from the measurements, especially at the last exposure period (Fig. 2H and Figs. S1H, S2H, S3H). The limited capacity of the model to simulate Cu accumulation in this fraction is attributable to several factors. Unlike the simulation in the model, metal accumulation in the MRG might follow a hyperbolic relationship, as also reported for metal binding to MTLP (Brown and Parsons, 1978; Roesijadi, 1980). Another explanation might be related to the time required for metal incorporation into inorganic granules (Brown, 1982; Vijver et al., 2004). Therefore, the use of one rate constant for irreversible detoxification as in the model might not appropriately describe the kinetic Cu accumulation in the MRG. A two-compartment PTM for slow and quick detoxification via incorporation in the MRG might be considered to improve the prediction accuracy.

The model was least sensitive to parameters related to Cu kinetics in the cellular debris. This result indicated the limited significance of this compartment in terms of toxicology, which is consistent with the findings of previous studies (Cain et al., 2004; Buchwalter et al., 2008). This fraction is usually excluded in models based on subcellular metal partitioning (Tan and Wang, 2012). Despite that, the present study demonstrated that this compartment should be considered as well. On the one hand, such an approach facilitates an estimation of the total internal concentration. On the other hand, the inclusion of metal accumulation in this fraction provides more accurate estimates of metal concentrations in other subcellular fractions. With a high transport rate from the MAP to the cellular debris compared to the backward flow (Table 1), metal accumulation in the cellular debris might play a role as a storage compartment, thus reducing the metal concentration in the MAP or the concentration of potentially toxic metal.

3.3. *Relationship between metal binding to sensitive fractions and metal toxicity*

In the last step of the causality chain, the model unraveled the sensitivity of the organism to changes in the Cu concentration in the PTM fraction. Experimental data demonstrated fluctuations in the GST activity (Fig. 2I–J and Figs. S1I-J, S2I-J, S3I-J) as well the LPO level (Fig. 2K-L and Figs. S1K-L, S2K-L, S3K-L) in Cu-exposed mussels. Although these fluctuations could not be completely covered, the difference in their overall trend could be explained by the model (Fig. 2I-J-K-L and Figs. S1I-J-K-L, S2I-J-K-L, S3I-J-K-L). According to the results of model calibration, the GST activity responded more strongly to changes in the concentration of potentially toxic Cu than LPO (Table 1). A higher damage accrual rate constant for GST stimulation resulted in slight increases in the GST activity (Fig. 2I–J and Figs. S1I-J, S2I-J, S3I-J), compared to more stable LPO (Fig. 2K-L and Figs. S1K-L, S2K-L, S3K-L). Such differences were also seen in the measured changes of these two biomarkers during the exposure. The GST activity is indicative of the counteract response against oxidative stress-induced damages through

the conjugation with glutathione (Wang et al., 2012). Therefore, the stronger response in terms of the GST activity than the LPO level demonstrates the capacity of the Zebra mussel to limit oxidative stress-caused damages. In combination with the recovery of the antioxidant defence system, a slight increase in the GST activity prevented oxidative stress-induced damages as shown by the stability of the LPO level over time (Fig. 2K-L and Figs. S1K-L, S2K-L, S3K-L). These results proved that mechanisms of toxicity could be explained by the model, although the calibration results unraveled uncertainties inherent in the current approach for liking biomarker responses to the concentration of potentially toxic metal (Table 1).

Although it has been suggested that metal toxicity is related to metal concentrations at sites of toxic action, it remains challenging to quantify or to estimate this predictor. In dynamic models developed previously for acute toxicity, adverse effects were assumed to occur when the uptake rate exceeds the combination of detoxification and elimination rates (Van Straalen et al., 2005; Rainbow, 2007; Luoma and Rainbow, 2008; Casado-Martinez et al., 2010; Rainbow and Luoma, 2011a). However, Giguere et al. (2006) revealed that there is no threshold below which no metal accumulation in sensitive fractions occurs. In other words, metals are built up in sensitive fractions even when detoxification mechanisms are still able to sequester excess metals further. This is in accordance with the present study, as Cu was already found in the organelle and HSP fraction of mussels prior to the experiment. Therefore, it is evident that there was no threshold below which this metal could be successfully detoxified.

4. Conclusions

The TK-TD model developed in the present study is the first one that allows for delineating a whole exposure-response causality chain by integrating various factors. Specifically, the influence of water chemistry was considered in simulating metal uptake as both the influence on metal availability (expressed by the free metal ion activity) and potential competition between cations for uptake sites are accounted for. In addition, the integration of subcellular metal partitioning enables theoretical estimation of the metal concentration in the fraction of potentially toxic metal. Furthermore, this indicator was assumed to appropriately represent the concentration of metals at sites of toxic action and to be directly related to the biological responses. In such estimation, all various pathways for chelation of internalised metals by subcellular ligands in metabolism, detoxification, and elimination were taken into consideration. In the present study, the model was calibrated with simplified experimental conditions. However, its framework is theoretically applicable to other conditions, other aquatic organisms, and other metals as well. Further calibration is required to reduce uncertainties in model estimation, especially for the TD phase. The model should be validated with more environmentally relevant conditions, for example, with organic matter additions and with natural waters.

Declaration of competing interest

The authors declare that they have no known competing financial interests or personal relationships that could have appeared to influence the work reported in this paper.

Acknowledgements

We would like to thank the Deutsche Forschungsgemeinschaft (DFG), Germany, for granting the project (LE3716/2–1).

Appendix A. Supplementary data

Supplementary data to this article can be found online at https://doi.org/10.1016/j.chemosphere.2021.131930.

Author statement

T.T. Yen Le: Conceptualisation, Methodology, Investigation, Validation, Visualization, Writing, Funding acquisition, **Nachev Milen:** Methodology, Investigation, Reviewing and Editing, **Daniel Grabner:** Methodology, Investigation, Reviewing and Editing, **A. Jan Hendriks:** Validation, Reviewing and Editing, **Willie J.G.M. Peijnenburg:** Methodology, Validation, Reviewing and Editing, **Bernd Sures:** Project administration, Validation, Reviewing and Editing.

References

Allen, H.E., Hall, R.H., Brisbin, T.D., 1980. Metal speciation. Effects on aquatic toxicity. Environ. Sci. Technol. 14, 441–443.
Amiard, J.-C., Amiard-Triquet, C., Barka, S., Pellerin, J., Rainbow, P.S., 2006. Metallothioneins in aquatic invertebrates: their role in metal detoxification and their use as biomarkers. Aquat. Toxicol. 76, 160–202.
Ashauer, R., Escher, B.I., 2010. Advantages of toxicokinetic and toxicodynamic modelling in aquatic ecotoxicology and risk assessment. J. Environ. Monit. 12, 2056–2061.
Ashauer, R., Boxall, A.B.A., Brown, C.D., 2007. New ecotoxicological model to simulate survival of aquatic invertebrates after exposure to fluctuating and sequential pulses of pesticides. Environ. Sci. Technol. 41, 1480–1486.
Ashauer, R., Thorbek, P., Warinton, J.S., Wheeler, J.R., Maund, S., 2013. A method to predict and understand fish survival under dynamic chemical stress using standard ecotoxicity data. Environ. Toxicol. Chem. 32, 964–965.
Balsa-Canto, E, Alonso, A.A, Banga, J.R, 2010. An iterative identification procedure for dynamic modeling of biochemical networks. BMS Syst. Biol. 4, 11.
Balsa-Canto, E., Henriques, D., Gabor, A., Banga, J.R., 2016. AMIGO2, a toolbox for dynamic modeling, optimization and control in systems biology. Bioinformatics. https://doi.org/10.1093/bioinformatics/btw411.
Blackmore, G., Wang, W.-X., 2002. Uptake and efflux of Cd and Zn by the green mussel *Perna viridis* after metal preexposure. Environ. Sci. Technol. 36, 989–995.
Blanchard, J., Brix, K., Grosell, M., 2009. Subcellular fractionation of Cu exposed oyster, *Crassostrea virginica*, and Cu accumulation from a biologically incorporated Cu rich oyster diet in *Fundulus heteroclitus* in fresh and sea water. Comp. Biochem. Physiol., C 149, 531–539.
Brouwer, M., Syring, R., Brouwer, T.H., 2002. Role of a copper-specific metallothionein of the blue crab, *Callinectes sapidus*, in copper metabolism associated with degradation and synthesis of hemocyanin. J. Inorg. Biochem. 88, 228–239.
Brown, B.E., 1982. The form and function of metal-containing "granules" in invertebrate tissues. Biol. Rev. 57, 621–667.
Brown, D.A., Parsons, T.R., 1978. Relationship between cytoplasmic distribution of mercury and toxic effects to zooplankton and chum salmon (*Onchorhynchus keta*) exposed to mercury in a controlled ecosystem. J. Fish. Res. Board Can. 35, 880–884.
Buchwalter, D.B., Cain, D.J., Martin, C.A., Xie, L., Luoma, S.N., Garland Jr., T., 2008. Aquatic insect ecophysiological traits reveal phylogenetically based differences in dissolved cadmium susceptibility. Proc. Natl. Acad. Sci. U.S.A. 105, 8321–8326.
Cain, D.J., Luoma, S.N., Wallace, W.G., 2004. Linking metal bioaccumulation of aquatic insects to their distribution patterns in a mining-impacted river. Environ. Toxicol. Chem. 23, 1463–1473.
Campana, O., Taylor, A.M., Maher, W.A., Simpson, S.L., 2015. Importance of subcellular metal partitioning and kinetics to predicting sublethal effects of copper in two deposit-feeding organisms. Environ. Sci. Technol. 49, 1806–1814.
Campbell, P.G.C., 1995. Interactions between trace metals and aquatic organisms: a critique of the free-ion activity model. In: Tessier, A., Turner, D.R. (Eds.), Metal Speciation and Bioavailability in Aquatic Systems. John Wiley & Sons, Chichester, UK, pp. 45–102.
Casado-Martinez, M.C., Smith, B.D., Luoma, S.N., Rainbow, P.S., 2010. Metal toxicity in a sediment-dwelling polychaete: threshold body concentrations or overwhelming accumulation rates? Environ. Pollut. 158, 3071–3076.
Chis, O., Banga, J.R., Balsa-Canto, E., 2011. GenSSI: a software toolbox for structural identifiability analysis of biological models. Bioinformatics 27, 2610–2611.
Croteau, M.-N., Luoma, S.N., 2009. Predicting dietborne metal toxicity from metal influxes. Environ. Sci. Technol. 43, 4915–4921.
De Paiva Magalhaes, D., da Costa, M.R., Baptista, D.F., Buss, D.F., 2015. Metal bioavailability and toxicity in freshwaters. Environ. Chem. Lett. 13, 69–87.
De Schamphelaere, K.A.C., Janssen, C.R., 2002. A biotic ligand model predicting acute copper toxicity for *Daphnia magna*: the effects of calcium, magnesium, sodium, potassium, and pH. Environ. Sci. Technol. 36, 48–54.
De Schamphelaere, K.A.C., Stauber, J.L., Wilde, K.L., Markich, S.J., Brown, P.L., Franklin, N.M., Creighton, N.M., Janssen, C.R., 2005. Toward a biotic ligand model for freshwater green algae: surface-bound and internal copper are better predictions of toxicity than free Cu^{2+}-ion activity when pH is varied. Enviorn. Sci. Technol. 39, 2067–2072.
Di Toro, D.M., Allen, H.E., Bergman, H.L., Meyer, J.S., Paquin, P.R., Santore, R.C., 2001. Biotic ligand model of the acute toxicity of metals. 1. Technical basis. Environ. Toxicol. Chem. 20, 2383–2396.
Feng, J., Gao, Y., Chen, M., Xu, X., Huang, M., Yang, T., Chen, N., Zhu, L., 2018. Predicting cadmium and lead toxicities in zebrafish (*Danio rerio*) larvae by using a toxicokinetic-toxicodynamic model that considers the effects of cations. Sci. Total Environ. 625, 1584–1595.

Gao, Y., Feng, J., Zhu, L., 2015. Prediction of acute toxicity of cadmium and lead to zebrafish larvae by using a refined toxicokinetic-toxicodynamic model. Aquat. Toxicol. 169, 37–45.
Gao, Y., Feng, J., Zhu, L., 2017. Toxicodynamic modeling of zebrafish larvae to metals using stochastic death and individual tolerance models: comparisons of model assumptions, parameter sensitivity and predictive performance. Ecotoxicology 26, 295–307.
Gibbs, P.E., Nott, J.A., Nicolidou, A., Bebianno, M.J., 1998. The composition of phosphate granules in the digestive glands of marine prosobranch gastropods: variation in relation to taxonomy. J. Molluscan Stud. 64, 423–433.
Giguere, A., Campbell, P.G.C., Hare, L., Couture, P., 2006. Sub-cellular partitioning of cadmium, copper, nickel and zinc in indigenous yellow perch (*Perca flavescenes*) sampled along a polymetallic gradient. Aquat. Toxicol. 77, 178–189.
Gustafsson, J.P., 2011. Visual MINTEQ 3.0 User Guide. Royal Institute of Technology, Stockholm, Sweden.
Handy, R.D., Eddy, F.B., Baines, H., 2002. Sodium-dependent copper uptake across epithelia: a review of rationale with experimental evidence from gills and intestine. Biochim. Biophys. Acta 1566, 104–115.
He, E., Qiu, H., Van Gestel, C.A.M., 2014. Modelling uptake and toxicity of nickel in solution to *Enchytraeus crypticus* with biotic ligand model theory. Environ. Pollut. 188, 17–26.
Jager, T., Albert, C., Preuss, T.G., Ashauer, R., 2011. General unified threshold model of survival – a toxicokinetic-toxicodynamic framework for ecotoxicology. Environ. Sci. Technol. 45, 2529–2540.
Kalman, J., Bonnail-Miguel, E., Smith, B.D., Bury, N.R., Rainbow, P.S., 2015. Toxicity and the fractional distribution of trace metals accumulated from contaminated sediments by the clam *Scrobicularia plana* exposed in the laboratory and the field. Sci. Total Environ. 506 (507), 109–117.
Kamunde, C., 2009. Early subcellular partitioning of cadmium in gill and liver of rainbow trout (*Oncorhynchus mykiss*) following low-to-near-lethal waterborne cadmium exposure. Aquat. Toxicol. 91, 291–301.
Le, T.T.Y., Nachev, M., Grabner, D., Garcia, M.R., Balsa-Canto, E., Hendriks, A.J., Peijnenburg, W.J.G.M., Sures, B., 2021a. Modelling chronic toxicoinetics and toxicodynamics of copper in mussels considering ionoregulatory homeostasis and oxidative stress. Environ. Pollut. 287, 117645.
Le, T.T.Y., Peinenburg, W.J.G.M., Hendriks, A.J., Vijver, M.G., 2012. Predicting effects of cations on copper toxicity to lettuce (*Lactuca sativa*) by the biotic ligand model. Environ. Toxicol. Chem. 31, 355–359.
Le, T.T.Y., Grabner, D., Nachev, M., Peijnenburg, W.J.G.M., Hendriks, A.J., Sures, B., 2021b. Modelling copper toxicokinetics in the zebra mussel, *Dreissena polymrpha*, under chronic exposures at various pH and sodium concentrations. Chemosphere 267, 129278.
Ligon, T.S., Froehlich, F., Chis, O.T., Banga, J.R., Balsa-Canto, E., Hasenauer, J., 2018. GenSSI 2.0: multi-experiment structural identifiability analysis of SBML models. Bioinformatics 34, 1421–1423.
Luoma, S.N., Rainbow, P.S., 2008. Metal Contamination in Aquatic Environments. Science and Lateral Management. Cambridge University Press, Cambridge, UK.
Markl, J., 2013. Evolution of molluscan hemocyanin structures. Biochim. Biophys. Acta 1834, 1840–1853.
Morel, F.M.M., 1983. Principles of Aquatic Chemistry. Wiley Inter-Science, New York. NY, USA.
Ng, T.Y.-T., Wang, W.-X., 2005. Dynamics of metal subcellular distribution and its relationship with metal uptake in marine mussels. Environ. Toxicol. Chem. 24, 2365–2372.
Niyogi, S., Wood, C.M., 2004. Biotic ligand model, a flexible tool for developing site-specific water quality guidelines for metals. Environ. Sci. Technol. 38, 6177–6192.
Osterauer, R., Marschner, L., Betz, O., Gerberding, M., Sawasdee, B., Cloetens, P., Haus, N., Sures, B., Triebskorn, R., Koehler, H.-R., 2010. Turning snails into slugs: induced body plan changes and formation of an internal shell. Evol. Dev. 12, 475–483.
Pagenkopf, G.K., Russo, R.C., Thurston, R.V., 1974. Effect of complexation on toxicity of copper to fishes. J. Fish. Res. Board Can. 31, 462–465.
Pan, K., Wang, W.-X., 2008. The subcellular fate of cadmium and zinc in the scallop *Chlamys nobilis* during waterborne and dietary metal exposure. Aquat. Toxicol. 90, 253–260.
Paquin, P.R., Gorsuch, J.W., Apte, S., Batley, G.E., Bowles, K.C., Campbell, P.G.C., Delos, C.G., Di Toro, D.M., Dwyer, R.L., Galvez, F., Gensemer, R.W., Goss, G.C., Hogstrand, C., Janssen, C.R., McGeer, J.C., Naddy, R.B., Playle, R.C., Santore, R.C., Schneider, U., Stubblefield, W.A., Wood, C.M., Wu, K.B., 2002. The biotic ligand model: a historical overview. Comp. Biochem. Physiol., C 133, 3–36.
Peijnenburg, W., Sneller, E., Sijm, D., Lijzen, J., Traas, T., Verbruggen, E., 2002. Implementation of bioavailability in standard setting and risk assessment? J. Soils Sediments 2, 169–173.
Playle, R.C., 1998. Modelling metal interactions at fish gills. Sci. Total Environ. 219, 147–163.
Playle, R.C., Dixon, D.G., Burnison, K., 1993. Copper and cadmium binding to fish gills: estimates of metal-gill stability constants and modelling of metal accumulation. Can. J. Fish. Aquat. Sci. 50, 2678–2687.
Rainbow, P.S., 2002. Trace metal concentrations in aquatic invertebrates: why and so what? Environ. Pollut. 120, 497–507.
Rainbow, P.S., 2007. Trace metal bioaccumulation: models, metabolic availability and toxicity. Environ. Int. 33, 576–582.
Rainbow, P.S., Luoma, S.N., 2011a. Metal toxicity, uptake and bioaccumulation in aquatic invertebrates – modelling zinc in crustaceans. Aquat. Toxicol. 105, 455–465.
Rainbow, P.S., Luoma, S.N., 2011b. Trace metals in aquatic invertebrates. In: Beyer, W. N., Meador, J.P. (Eds.), Environmental Contaminants in Biota: Interpreting Tissue Concentrations. Taylor and Francis Books, Boca Raton, FL, USA, pp. 231–252.
Rainbow, P.S., Smith, B.D., 2013. Accumulation and detoxification of copper and zinc by the decapod crustacean *Palaemonetes varians* from diets of field-contaminated polychaetes *Nereis diversicolor*. J. Exp. Mar. Biol. Ecol. 449, 312–320.
Roesijadi, G., 1980. Influence of copper on the clam *Protothaca staminea*: effects on gills and occurrence of copper-binding proteins. Biol. Bull. 158, 233–247.
Serafim, A., Bebianno, M.J., 2007. Kinetic model of cadmium accumulation and elimination and metallothionein response in *Ruditapes decussatus*. Environ. Toxicol. Chem. 26, 960–969.
Slaveykova, V.I., Wilkinson, K.J., 2005. Predicting the bioavailability of metals and metal complexes: critical review of the biotic ligand model. Environ. Chem. 2, 9–24.
Sprague, J.B., 1968. Promising anti-pollutant: chelating agent NTA protects fish from copper and zinc. Nature 220, 1345–1346.
Sunda, W.G., Huntsman, S.A., 1998. Processes regulating cellular metal accumulation and physiological effects: phytoplankton as model systems. Sci. Total Environ. 219, 165–181.
Tan, Q.-G., Wang, W.-X., 2012. Two-compartment toxicokinetic-toxicodynamic model to predict metal toxicity in *Daphnia magna*. Environ. Sci. Technol. 46, 9709–9715.
Tipping, E., 1998. Humic ion-binding model VI: an improved description of the interactions of protons and metal ions with humic substances. Aquat. Geochem. 4, 3–48.
Van Straalen, N.M., Donker, M.H., Vijver, M.G., Van Gestel, C.A.M., 2005. Bioavailability of contaminants estimated from uptake rates into soil invertebrates. Environ. Pollut. 136, 409–417.
Veltman, K., Hendriks, A.J., Huijbregts, M.A.J., Wannaz, C., Jolliet, O., 2014. Toxicokinetic toxicodynamic modeling of Ag toxicity in freshwater organisms: whole-body sodium loss predicts acute mortality across aquatic species. Environ. Sci. Technol. 48, 14481–14489.
Vijver, M.G., van Gestel, C.A.M., Lanno, R.P., van Straalen, N.M., Peijnenburg, W.J.G.M., 2004. Internal metal sequestration and its ecotoxicological relevance: a review. Environ. Sci. Technol. 38, 4705–4712.
Wallace, W.G., Lopez, G.L., Levinton, J.S., 1998. Cadmium resistance in an oligochaete and its effect on cadmium trophic transfer to an omnivorous shrimp. Mar. Ecol. Prog. Ser. 162, 225–237.
Wallace, W.G., Lee, B.G., Luoma, S.N., 2003. Subcellular compartmentalization of Cd and Zn in two bivalves. I. Significance of metal sensitive fractions (MSF) and biologically detoxified meal (BDM). Mar. Ecol. Prog. Ser. 249, 183–197.
Wang, W.-X., 2013. Prediction of metal toxicity in aquatic organisms. Chin. Sci. Bull. 58, 194–202.
Wang, W.-X., Rainbow, P.S., 2006. Subcellular partitioning and the prediction of cadmium toxicity to aquatic organisms. Environ. Chem. 3, 395–399.
Wang, W.-X., Tan, Q.-G., 2019. Applications of dynamic models in predicting the bioaccumulation transport and toxicity of trace metals in aquatic organisms. Environ. Pollut. 252, 1561–1573.
Wang, Z., Yan, C., Vulpe, C.D., Yan, Y., Chi, Q., 2012. Incorporation of in situ exposure and biomarker response in clams *Ruditapes philippinarum* for assessment of metal pollution in coastal areas from the Maluan Basin of China. Mar. Pollut. Bull. 64, 90–98.
White, S.L., Rainbow, P.S., 1985. On the metabolic requirements for copper and zinc in molluscs and crustaceans. Mar. Environ. Res. 16, 215–229.